Proton cyclotron waves occurrence rate upstream from Mars observed by MAVEN: associated variability of the Martian upper atmosphere

Norberto Romanelli, Christian Mazelle, Jean-Yves Chaufray, Karim Meziane, Lican Shan, Suranga Ruhunusiri, Jack E. P. Connerney, Jared R. Espley, Francis Eparvier, Edward M. B. Thiemann, et al.

AGU PUBLICATIONS

JGR

Journal of Geophysical Research: Space Physics

RESEARCH ARTICLE
10.1002/2016JA023270

Special Section:
Major Results From the MAVEN Mission to Mars

Proton cyclotron waves occurrence rate upstream from Mars observed by MAVEN: Associated variability of the Martian upper atmosphere

N. Romanelli[1,2], C. Mazelle[1,2], J. Y. Chaufray[3], K. Meziane[4], L. Shan[5], S. Ruhunusiri[6], J. E. P. Connerney[7], J. R. Espley[7], F. Eparvier[8], E. Thiemann[8], J. S. Halekas[6], D. L. Mitchell[9], J. P. McFadden[9], D. Brain[8], and B. M. Jakosky[8]

[1]Institut de Recherche en Astrophysique et Planétologie, CNRS, Toulouse, France, [2]Institut de Recherche en Astrophysique et Planétologie, Paul Sabatier University, Toulouse, France, [3]Laboratoire Atmosphere, Milieux et Observations Spatiales (LATMOS), IPSL, CNRS, UVSQ, UPMC, Guyancourt, France, [4]Department of Physics, University of New Brunswick, Fredericton, New Brunswick, Canada, [5]Institute of Geology and Geophysics, Chinese Academy of Sciences, Beijing, China, [6]Department of Physics and Astronomy, University of Iowa, Iowa City, Iowa, USA, [7]NASA Goddard Space Flight Center, Greenbelt, Maryland, USA, [8]Laboratory for Atmospheric and Space Physics, University of Colorado Boulder, Boulder, Colorado, USA, [9]Space Sciences Laboratory, University of California, Berkeley, California, USA

Abstract Measurements provided by the Magnetometer and the Extreme Ultraviolet Monitor (EUVM) on board the Mars Atmosphere and Volatile EvolutioN (MAVEN) spacecraft together with atomic H exospheric densities derived from numerical simulations are studied for the time interval from October 2014 up to March 2016. We determine the proton cyclotron waves (PCWs) occurrence rate observed upstream from Mars at different times. We also study the relationship with temporal variabilities of the high-altitude Martian hydrogen exosphere and the solar EUV flux reaching the Martian environment. We find that the abundance of PCWs is higher when Mars is close to perihelion and decreases to lower and approximately constant values after the Martian Northern Spring Equinox. We also conclude that these variabilities cannot be associated with biases in MAVEN's spatial coverage or changes in the background magnetic field orientation. Higher H exospheric densities on the Martian dayside are also found when Mars is closer to perihelion, as a result of changes in the thermospheric response to variability in the ultraviolet flux reaching Mars at different orbital distances. A consistent behavior is also observed in the analyzed daily irradiances measured by the MAVEN EUVM. The latter trends point toward an increase in the planetary proton densities upstream from the Martian bow shock near perihelion. These results then suggest a method to indirectly monitor the variability of the H exosphere up to very high altitudes during large time intervals (compared to direct measurements of neutral particles), based on the observed abundance of PCWs.

Key Points:
- First confirmation that PCWs abundance upstream from the Martian bow shock varies with time, with higher values near perihelion
- At higher altitudes, temporal variabilities in the dayside exospheric H density display a similar long-term trend
- Exospheric variability partly caused by solar UV forcing on the thermosphere; water vapor might also contribute

Correspondence to:
N. Romanelli,
nromanelli@irap.omp.eu

Citation:
Romanelli, N., et al. (2016), Proton cyclotron waves occurrence rate upstream from Mars observed by MAVEN: Associated variability of the Martian upper atmosphere, *J. Geophys. Res. Space Physics*, *121*, 11,113–11,128, doi:10.1002/2016JA023270.

Received 2 AUG 2016
Accepted 8 NOV 2016
Accepted article online 15 NOV 2016
Published online 25 NOV 2016

1. Introduction

For planets lacking an intrinsic global dynamo-generated magnetic field such as Mars [*Acuña et al.*, 1998], the presence of a neutral exosphere that extends beyond their bow shock (BS) [*Chaufray et al.*, 2008; *Chaffin et al.*, 2015] has significant consequences for the physical processes taking place when interacting with the solar wind (SW) [e.g., *Mazelle et al.*, 2004]. In particular, the interaction between the Martian atmosphere and the SW starts upstream from the BS (standoff distance ~1.6 R_M from the center of Mars) where particles from the extended exosphere (mainly atomic hydrogen) are ionized and picked up (Larmor radius of a newborn planetary proton ~0.3 R_M) several planetary radii away from the planet [e.g., *Yamauchi et al.*, 2015].

As a result of different ionization processes affecting the Martian hydrogen (H) exosphere and the relative velocity between the H atoms and the SW, the proton velocity distribution function at these altitudes (seen from the SW reference frame) is composed by a core of SW particles and a nonthermal population associated with the presence of newborn planetary ions. This type of particle velocity distribution functions has been shown to be highly unstable [*Wu and Davidson*, 1972; *Wu and Hartle*, 1974; *Tsurutani et al.*, 1989; *Tsurutani*, 1991; *Brinca*, 1991; *Gary*, 1991; *Mazelle and Neubauer*, 1993; *Sauer et al.*, 2001; *Sauer and Dubinin*, 2003; *Cowee et al.*, 2012] and capable of giving rise to different ultralow-frequency electromagnetic plasma wave modes.

However, despite the capability of exciting different wave modes [*Gary*, 1993; *Brinca and Tsurutani*, 1989; *Convery and Gary*, 1997; *Gary and Madland*, 1988; *Gary et al.*, 1989] (depending on several parameters, for example, the value of the angle between the background magnetic field and the SW velocity direction at the time of the proton pickup, i.e., the interplanetary magnetic field (IMF) cone angle), the frequency of these waves, observed from the newborn planetary proton reference frame, is very close to the local proton cyclotron frequency [*Brinca*, 1991]. This observation (also valid in the planetary reference frame itself and also for observations from spacecraft (SC) moving around the planet with velocities of a few km s^{-1}) results from the fact that the initial velocity of the newborn protons with respect to the atmospheric planet is negligible compared to the SW flow velocity, as it is also the case for the spacecraft's velocity range. In other words, despite the possibility of exciting different plasma wave modes by means of the implantation of planetary protons into the SW, the Doppler shift associated with the relative velocity between the associated newborn proton population and the SW is responsible for the observation of waves at the local proton cyclotron frequency in the SC reference frame. These waves are called proton cyclotron waves or PCWs.

PCWs upstream from the Martian bow shock have been reported and studied through magnetic field measurements obtained thanks to different spacecraft [*Russell et al.*, 1990; *Brain et al.*, 2002; *Mazelle et al.*, 2004; *Wei and Russell*, 2006; *Romanelli et al.*, 2013; *Bertucci et al.*, 2013; *Wei et al.*, 2011, 2014; *Connerney et al.*, 2015a; *Ruhunusiri et al.*, 2015, 2016]. All these studies have identified waves at the local proton cyclotron frequency left-handed polarized (in the SC frame) that propagate quasi-parallel with respect to the IMF.

Among these works, *Romanelli et al.* [2013] reported the presence of a strong difference in the occurrence rate of PCWs between two different premapping subphases of the Mars Global Surveyor (MGS) mission. The authors suggested that these changes do not seem to be related with changes in the IMF cone angle and MGS spatial coverage since the statistical distribution of the former parameter and the altitude range did not change significantly between both subphases. After this work, *Bertucci et al.* [2013] analyzed the PCWs occurrence rate in the upstream region of Mars for all MGS premapping orbits. They based their study on the characteristic property of the PCWs, i.e., a peak in the power spectral density (PSD) of the transverse component of the magnetic field at the local proton cyclotron frequency. Also, in order to ensure a common altitude coverage, they focused their study on MGS magnetic field measurements obtained at altitudes below 20,400 km (i.e., ~6 R_M, where R_M stands for Martian radius). The analyses of such observations, obtained at high southern latitudes during minimum to mean solar activity, showed that the PCWs occurrence rate is significantly higher around the Martian perihelion (close to the Southern Summer Solstice) than around the spring and autumn equinoxes. Assuming that the ionization frequencies of the exospheric H neutral atoms remained constant during the whole studied time interval, these authors also explored if temporal changes in the Martian atomic H corona extent could be the reason for the observed long-term variability in the PCWs occurrence rate. By means of numerical simulations, *Bertucci et al.* [2013] found that the H density profiles over the Martian dayside and south pole exhibited a similar long-trend temporal behavior to that of the PCWs occurrence rate, suggesting then a coupling between the variability of the Martian H exosphere and excitation of these electromagnetic plasma waves.

Related studies focused on the temporal variabilities of the neutral and ionized environment of Mars over a Martian year or longer can be found in *Chaufray et al.* [2015], in *Yamauchi et al.* [2015] (based on Mars Express data), and in *Brain et al.* [2005] (based on MGS data). The variability of the exospheric atomic H density and H escape resulting from changes in the Martian orbital location as well as the solar activity has been studied in detail in *Chaufray et al.* [2015]. Variabilities in the plasma properties of the Martian environment upstream from the bow shock have been reported in *Yamauchi et al.* [2015]. These authors reported a strong correlation between the detection frequency of pickup ions originating from newly ionized exospheric hydrogen and the Sun-Mars distance, displaying changes every Martian year, approximately. Higher detection rate of pickup ions were observed when Mars is around perihelion. *Yamauchi et al.* [2015] arrived at this conclusion by analyzing Mars Express Ion Mass Analyzer observations obtained in the upstream region of Mars during 8 Earth years. PCWs observations could not be obtained from this spacecraft since its payload did not contain a magnetometer. Spatial regions inside the induced magnetosphere of Mars have also been shown to present seasonal changes. Indeed, based on electron energy spectra taken from more than 5 Earth years of MGS during the mapping phase, *Brain et al.* [2005] concluded that the Martian magnetic pileup boundary (MPB) position is sensitive to the Martian orbital location, such that the MPB is closer to the planet when Mars is near its aphelion.

In the present work we first investigate whether the previously reported long-term temporal variability in the PCWs occurrence rate upstream from Mars is confirmed by magnetometer (MAG) observations obtained during the MAVEN mission [*Jakosky et al.*, 2015]. Thanks to the high accuracy of the magnetic field measurements, we are able to apply more strict criteria that consider not only the frequential but also the polarization properties of PCWs, allowing to gain more confidence in the presented results. Moreover, MAVEN measurements obtained around orbital apoapsis and upstream from the bow shock are not restricted to locations over the south pole of Mars, as it was the case of MGS highly elliptical premapping orbits [*Albee et al.*, 2001]. Indeed, after Mars orbit insertion (on 21 September 2014), MAVEN was placed in elliptical orbits with a period of 4.5 h, a periapsis altitude of ∼150 km, and an apoapsis altitude of ∼6200 km. MAVEN's orbit is inclined by 74° with respect to Mars's equatorial plane and precesses so that apoapsis (and therefore periapsis) occur at a wide range of latitudes and local times. Additionally, we numerically study the temporal variability of the Martian H exosphere for altitudes higher than that of MAVEN's spatial coverage. Indeed, the H exosphere is the main reservoir for upstream pickup protons and the PCWs observed by MAVEN are generated upstream from the detection region, since time and space is needed for the waves to grow and to be mainly convected by the SW (since both the phase and the group velocity of these low-frequency plasma waves are much lower than the SW speed). Due to the altitude range under consideration, numerical simulations for the H exospheric density are performed, for solar mean conditions and taking the orbital position of Mars around the Sun into account. Moreover, we also analyze the extreme ultraviolet measurements (EUV) obtained by the EUV monitor (EUVM) on board MAVEN during this time interval as it can affect the H exospheric structure and the photoionization frequencies of these neutral atoms. A comparison between the temporal variability of the MAVEN EUVM irradiance measurements and the abundance of PCWs and the derived simulation results (H densities) is performed.

The present study is structured as follows. In section 2 we briefly describe the capabilities of the MAVEN MAG and MAVEN EUVM instruments and the atmospheric numerical simulation model. In section 3 we present an example of a detected PCW event and the selection criteria applied for the statistical study of the MAG data set. Section 4 describes the MAVEN spatial coverage in the time interval under study. Section 5 contains the results of the analysis of the abundance of the PCWs and the temporal variability of the H exospheric density. Measurements of the EUVM are also interpreted in this section. Finally, the discussion of the results is developed in section 6, and our conclusions are presented in section 7.

2. Description of MAVEN Instruments and Adopted Numerical Simulation Code

2.1. The MAVEN Magnetometer (MAG)

The MAG instrument is a fluxgate magnetometer that provides vector magnetic field measurements over a broad range (to 65,536 nT per axis) for three axes with sampling frequency of 32 Hz and accuracy of 0.25 nT [*Connerney et al.*, 2015b]. For a mean IMF in the upstream region of Mars whose magnitude is ∼4 nT, the PCWs have a frequency of ∼0.06 Hz in the SC frame, that is, much lower than the MAG sampling frequency. Therefore, we have calculated 4 Hz averages of the MAG data since the Nyquist frequency (2 Hz) is still one order of magnitude larger than the expected PCWs frequency.

2.2. The MAVEN Extreme Ultraviolet Monitor (EUVM)

The EUVM instrument measures the variability of the solar soft X-rays and the EUV irradiance reaching Mars. MAVEN EUVM consists of three broadband radiometers, which allow the instrument to sample three solar EUV bands with a cadence of 1 s [*Eparvier et al.*, 2015]. Because we are interested in temporal changes on much larger temporal scales, in this work we consider daily irradiance averages in the 121–122 nm wavelength range, as this is mainly the most intense signal, when compared to the other two bands.

2.3. Three-Dimensional Exospheric-LMD-GCM Model

The three-dimensional structure of the high-altitude Martian H corona has been studied based on MAVEN Imaging Ultraviolet Spectrograph observations obtained during MAVEN's 35 h insertion orbit [*Chaffin et al.*, 2015]. For the purpose of the present study, however, estimations of the exospheric H densities at altitudes higher than MAVEN spatial coverage during the time interval under study are needed. Therefore, H densities obtained in this study are derived using a 3-D exospheric model detailed in *Chaufray et al.* [2012, 2015], taking into account the nonuniform spatial distribution of H densities and temperatures at the exobase given by the 3-D Laboratoire de Météorologie Dynamique Global Climate Model (LMD-GCM) model [*González-Galindo et al.*, 2009a; *Chaufray et al.*, 2015]. The LMD-GCM describes the hydrogen cycle from the water photodissociation in the lower atmosphere to the escape at the exobase assuming Jeans escape only [*Chaufray et al.*, 2015].

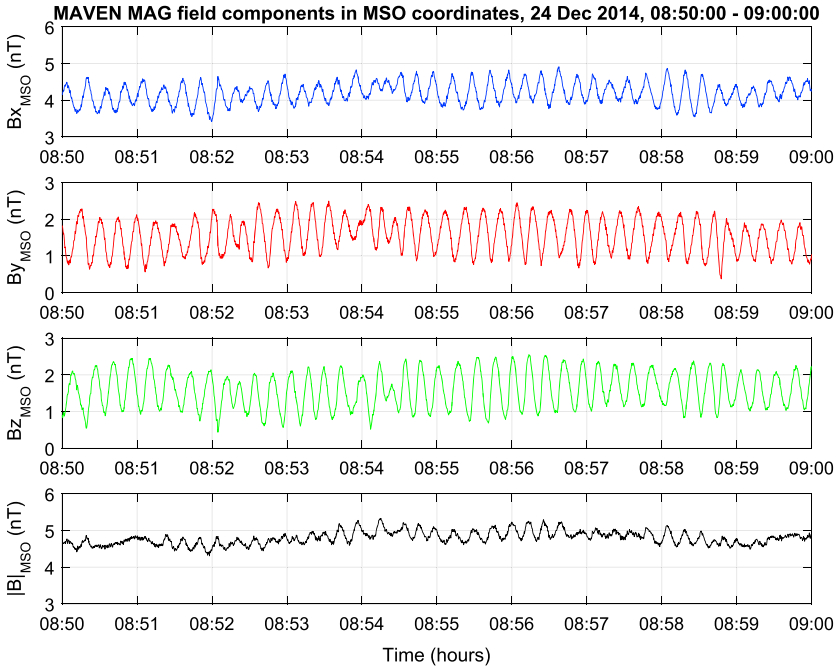

Figure 1. Magnetic field components and magnitude in MSO coordinates, for 24 December 2014, 08:50:00 UT–09:00:00 UT by MAVEN MAG in the upstream region of Mars (4 Hz averaged resolution).

A new simulation is performed for this study assuming a constant solar average scenario ($F_{10.7} \sim 120$) for the full Martian year. The solar activity regimes defined in the LMD-GCM are described in detail in *González-Galindo et al.* [2005].

3. PCWs: A Case Study and the MAG Selection Criteria

3.1. Case Study: A PCW Event on 24 December 2014

Figure 1 shows an example of a proton cyclotron wave event detected by MAVEN MAG upstream from the Martian bow shock. The measurements were obtained on 24 December 2014 during a 10 min window from 08:50 to 09:00 UT and are displayed (with a sampling frequency of 4 Hz) in the Mars-centered Solar Orbital (MSO) coordinates. The MSO coordinate system is defined as follows: the *X* axis points toward the Sun; the *Z* axis is perpendicular to Mars's orbital plane and is positive toward the ecliptic north. The *Y* axis completes the right-handed system.

The first three panels show the MSO magnetic field components, the fourth one displays the magnetic field magnitude. The mean magnetic field vector for this 10 min window is $\mathbf{B}_0$ = [4.19, 1.55, 1.59] nT and makes an angle of 152° with the nominal SW velocity vector, which for simplicity we take along the line Sun-Mars. All magnetic field components display oscillations with a well-defined frequency and amplitude around 0.5 nT. The compressive component has a lower amplitude (0.25 nT for $|\mathbf{B}_0| = 4.74$ nT). The associated proton cyclotron frequency (f_c) is 0.0723 Hz; i.e., the proton gyroperiod is 13.84 s.

We now calculate the power spectral density (PSD) for the transverse and compressive components with respect to $\mathbf{B}_0$, as shown by the blue and black lines in Figure 2, respectively. The vertical dashed line is located at the mean local proton cyclotron frequency (0.0723 Hz), and the black bar indicates the frequency range from 0.8 f_c up to 1.2 f_c, taking also the MAG uncertainty into account. The orange bars indicate a frequency interval of width 0.2 f_c, adjacent to the PCW frequency interval, and are not associated with PCWs. The adjacent intervals are used to determine if the PSD signatures are consistent with our selection criteria for PCWs (see next section). The peak in the PSD of the transverse component is located at 0.0716 Hz ($=0.99\,f_c$) and ~76 times higher than that for the compressive component at that frequency. Therefore, we conclude that the oscillations in Figure 1 have a frequency almost exactly at the local proton cyclotron frequency and take place mainly in the perpendicular plane to $\mathbf{B}_0$.

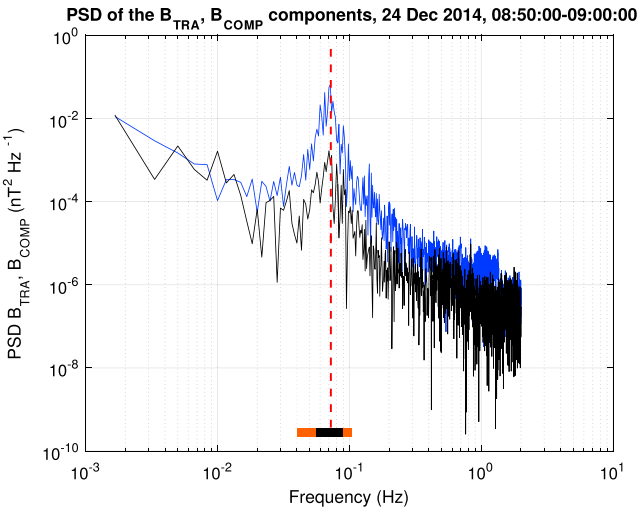

Figure 2. Power spectral density of the transverse (blue) and compressive (black) magnetic field components for 24 December 2014, 08:50:00 UT–09:00:00 UT for a case of positive detection of PCWs. The dashed line indicates the mean local proton cyclotron frequency, while the black segment displays the frequency range from $0.8\,f_c$ to $1.2\,f_c$, taken also into account the frequency uncertainty deriving from that of MAG (0.25 nT). Orange segments display the neighboring frequency ranges (not associated with waves at the local proton cyclotron frequency) where no significant intensity (compared to PSD peak at approximately f_c) can be seen.

By means of the Minimum Variance Analysis (MVA) [*Sonnerup and Scheible*, 1998] technique, we are able to provide an estimate for the direction of propagation (**k**) for the observed waves, assuming they are planar. To do this, we first calculate the eigenvalues of the covariance matrix of the magnetic field for different subintervals (corresponding to three local proton cyclotron gyroperiods approximately) within each 10 min window under study. The maximum, intermediate and minimum eigenvalues are denoted as λ_1, λ_2, and λ_3, respectively. The direction of the wave vector **k** is then approximated by that of the eigenvector $\mathbf{e}_3$ associated with the smallest eigenvalue, and the hypothesis that the waves are planar can be characterized by means of the λ_2/λ_3 ratio (which is larger for planar waves).

Figure 3 shows the result of the MVA on MAG data for the subinterval [08:55:24–08:56:04] UT. The left and right panels show the hodogram in the maximum-intermediate and intermediate-minimum planes, respectively. The mean magnetic field expressed in the MVA basis ($\mathbf{e}_1, \mathbf{e}_2, \mathbf{e}_3$) is $\mathbf{B}_0$ = [−0.76, 0.71, −4.74] nT and therefore points out of the maximum-intermediate plane as shown in the left panel. Moreover, the sense of gyration of the magnetic field oscillations (black arrow, left panel) with respect to $\mathbf{B}_0$ indicates then that the polarization, in the SC frame, is left handed. These waves are almost circularly polarized ($\lambda_1/\lambda_2 = 1.3$) and planar ($\lambda_2/\lambda_3 = 39.8$). Additionally, the angle θ_{kB} between the estimated wave propagation direction $\mathbf{e}_3$ and $\mathbf{B}_0$ is equal to 12.4°, indicating that these waves are propagating quasi-parallel to the mean magnetic field.

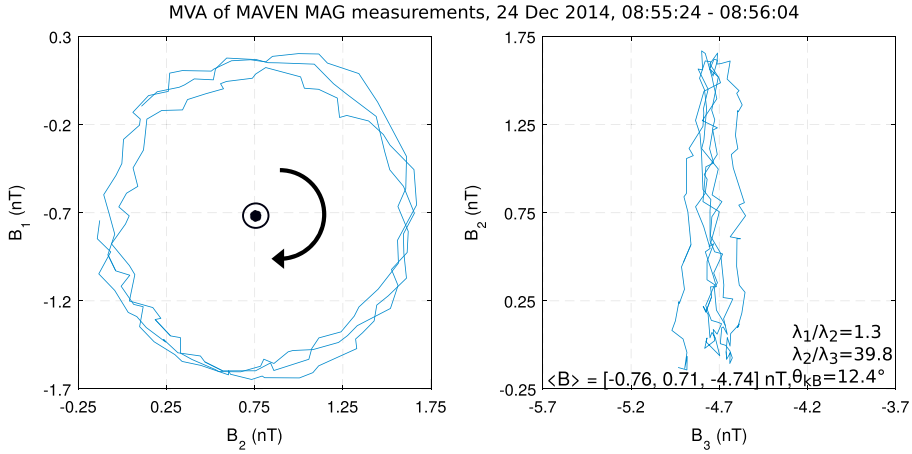

Figure 3. Minimum Variance Analysis of the MAVEN MAG field measurements for 24 December 2014, 08:55:24 UT–08:56:04 UT (4 Hz averaged). This time interval corresponds to three local proton cyclotron periods, approximately. The associated eigenvalues ratio are $\lambda_1/\lambda_2 = 1.3$ and $\lambda_2/\lambda_3 = 39.8$, the mean magnetic field (in the MVA basis) is $\mathbf{B}$ = [−0.76, 0.71, −4.74] nT, the polarization is left handed, and the propagation angle is $\theta_{kB} = 12.4°$.

In summary, all derived properties from Figures 2 and 3 are in full agreement with previously reported properties on PCWs [*Russell et al.*, 1990; *Brain et al.*, 2002; *Mazelle et al.*, 2004; *Wei and Russell*, 2006; *Romanelli et al.*, 2013; *Bertucci et al.*, 2013; *Wei et al.*, 2011, 2014; *Connerney et al.*, 2015a; *Ruhunusiri et al.*, 2015, 2016]. However, in order to determine the abundance of these waves as a function of time, we first need to clearly specify what properties will be analyzed when MAVEN MAG 10 min window measurements in the upstream region of Mars are being studied.

3.2. PCWs Selection Criteria for MAG Data

We now perform a statistical study in the upstream region of Mars for the time interval from October 2014 up to March 2016, i.e., 18 months or 0.79 times the Martian orbital period. During this time interval, Mars reached perihelion (PH) on 12 December 2014 and aphelion (APH) on 20 November 2015. The upstream region is defined using the Martian bow shock model from *Vignes et al.* [2000]. To determine the PCW occurrence rate as a function of time, we use two sets of criteria to decide if a PCW event has been detected. The analysis is performed on 10 min intervals, where we require that the mean magnetic field magnitude be 1.5 nT or larger in order to have a well determined local proton cyclotron frequency.

The first set of criteria is based on the PSD calculations for the 10 min data intervals. A PCW event is detected when the following occur:

1. The power spectral density of the transverse component displays an increase in a frequency interval centered around the local proton cyclotron frequency when compared to two contiguous windows. More precisely,

$$\mathrm{PSD}\left[B_{\perp}(f)\right]_{0.8f_c-\Delta f}^{1.2f_c+\Delta f} > \mathrm{PSD}\left[B_{\perp}(f)\right]_{1.2f_c+\Delta f}^{1.4f_c+\Delta f}, \mathrm{PSD}\left[B_{\perp}(f)\right]_{0.6f_c-\Delta f}^{0.8f_c-\Delta f} \quad (1)$$

   where Δf is the uncertainty in f_c associated with MAG's uncertainty (0.25 nT). Also, the PSD of the transverse component of the magnetic field measurements must be higher than that of for the compressive component, more specifically,

2.

$$\mathrm{PSD}\left[B_{\perp}(f)\right]_{f_c} > 3\,\mathrm{PSD}\left[B_{\mathrm{comp}}(f)\right]_{f_c} \quad (2)$$

   Each spectrum has been calculated using a Hanning window which reduces the spectral leakage, in addition to having a narrow main lobe.

   The second, more strict set of criteria, is in addition to the first and considers the polarization properties derived from an MVA analysis. A PCW event is detected when also the following occur:

3. The waves can be considered to be planar. From the MVA (applied on subintervals of three local proton cyclotron periods), we require that the λ_2/λ_3 ratio averaged over the 10 min window be equal or larger than 5.
4. The observed polarization in the SC frame is left handed. From the MVA (applied on subintervals of three local proton cyclotron periods), we require that the projection of $\mathbf{B}_0$ along $\mathbf{e}_3$ be opposite to the mean rotation vector of the magnetic field component in the $(\mathbf{e}_1, \mathbf{e}_2)$ plane averaged over the 10 min window.

We have performed these calculations for every 10 min MAG data window in the upstream region of Mars along the trajectory of MAVEN with a window overlapping of 90%.

The justification for applying these two sets of selection criteria is the following. The detection of a peak in the PSD at or close to the local proton cyclotron frequency (in the SC frame) implies that the magnetic field perturbations taking place during a particular 10 min interval display one of the key observational signatures expected for electromagnetic plasma waves excited the newborn planetary protons. However, all waves producing a peak around the local proton cyloctron frequency in the PSD spectrum, a priori, do not necessarily have a planar hodogram and a left-hand polarization in the SC frame. This is the case, for example, for dispersive wave packets produced by steepening of very low frequency compressive nonlinear waves which may have frequencies accidentally close to the proton cyclotron frequency (see, for instance, the discussion in *Mazelle and Neubauer* [1993, and references therein]). Moreover, MAVEN observes also nonlinear waves which keep the main signature around the local proton cyclotron frequency. Even though the source of these waves is also the newborn planetary protons, they are in a much more evolved stage than the monochromatic ones; that is, more time is needed to reach this state. Thus, since the waves are convected toward the planet

by the SW, they are observed at locations even much farther away from the proton source than the monochromatic PCWs. Therefore, they are less representative of the local neutral H corona. Based on these points, it is clear that the results derived based solely on PSD signatures allow us to provide the maximum value that the proton cyclotron wave occurrence rate can reach at a certain time interval, while the additional consideration of the polarization properties allows to provide the occurrence rate of events that fulfilled all the expected properties for PCWs that can be measured with MAVEN MAG.

It is also important to point out that a test of the sensitivity of our PCWs selection criteria has been applied to typical background magnetic field turbulent spectra (no PCWs signatures) to which an artificial quasi-monochromatic signal at the local proton cyclotron frequency is superimposed. These tests confirm that our sets of selection criteria are highly effective, capable of detecting waves at the local proton cyclotron frequency with amplitudes as low as ~0.02 nT.

4. Spatial Coverage of the Upstream Region of Mars by MAVEN: October 2014 to March 2016

Before determining the PCWs occurrence rate as a function of time, it is important to briefly describe MAVEN's spatial coverage of the upstream region of Mars, as well as to be aware of a possible bias in our calculations. Since properties of the exosphere change with radial distance from the planet, the SC altitude must be taken into account. The SC's orbital coverage in the $X_{MSO}-$ direction is important since PCWs are convected by the SW mainly along this direction. Furthermore, the coverage in the northern and southern MSO hemispheres (Z_{MSO}) is important to detect any effect of the crustal fields, which have highest magnitude in the southern hemisphere.

Figure 4 displays MAVEN spatial coverage of the region upstream from the Martian bow shock projected in MSO coordinates during the full time interval (10 October 2014 to 31 March 2016). Each point (in blue) corresponds to the mean position of an analyzed 10 min MAG window. Figure 4 (first to fourth panels) shows the SC altitude and the three MSO coordinates, as a function of time. Empty time intervals indicate that MAVEN was not in the upstream region or MAG was not active. A 3-D representation of these points in MSO coordinates (seen from two different view points) is also shown in Figure 4 (bottom panels), together with the trajectory of MAVEN during almost 2 days of the mission (in black).

Figure 4 (first panel) shows that MAVEN spanned a constant altitude range between 0.76 R_M and 1.91 R_M over the 18 months. The range in the X_{MSO} coordinate is restricted from near the terminator plane to 2.5 R_M toward the Sun. However, the range in Y_{MSO} and Z_{MSO} is more variable: from October 2014 to mid-March 2015, the spanned Y_{MSO} interval is $[-2.66, 1.37]$ R_M and the Z_{MSO} coordinate is mainly negative (southern hemisphere); from June 2015 to mid-October 2015 the Y_{MSO} and Z_{MSO} coordinates are both mainly positive (northern hemisphere); and from mid-December 2015 to March 2016 the Y_{MSO} coordinate is mainly positive and Z_{MSO} is again negative (southern hemisphere). During this time interval Mars went through several seasons. After reaching perihelion (1.38 AU) on 12 December 2014, the Northern Winter Solstice-Southern Summer Solstice (NWS-SSS) and Northern Spring Equinox-Southern Autumn Equinox (NSE-SAE) took place on 11 January 2015 and 18 June 2015, respectively. Later, Mars reached aphelion (1.67 AU), and the Northern Summer Solstice-Southern Winter Solstice (NSS-SWS) on 20 November 2015 and 3 January 2016, respectively. To provide an additional reference, the spatial distribution of the analyzed MAG windows in MSO coordinates is also shown in Figure 4 (bottom panels), which also displays, as an example, the SC trajectory (in black) during ~11 elliptical orbits that took place one day before to one day after the time interval analyzed in Figure 1. Red curves display the intersection of the Martian bow shock model [*Vignes et al.*, 2000] with the $Z_{MSO} = 0$ and $Y_{MSO} = 0$ planes.

5. Long-Term Variability of PCW Occurrence Rate, Exopsheric H Corona, and EUV Solar Flux

Figure 5 shows the PCWs occurrence rate as a function of time, based on the selection criteria specified in section 3. First, Figure 5 (top) displays three superimposed histograms with the number of 10 min intervals studied in the upstream region of Mars as a function of time, for bins of 15 terrestrial days width. This time width allows to study the long-term temporal variability in the abundance of the PCWs and is consistent with the temporal scales over which the planetary pickup ion detection rate (the source of these waves) have been

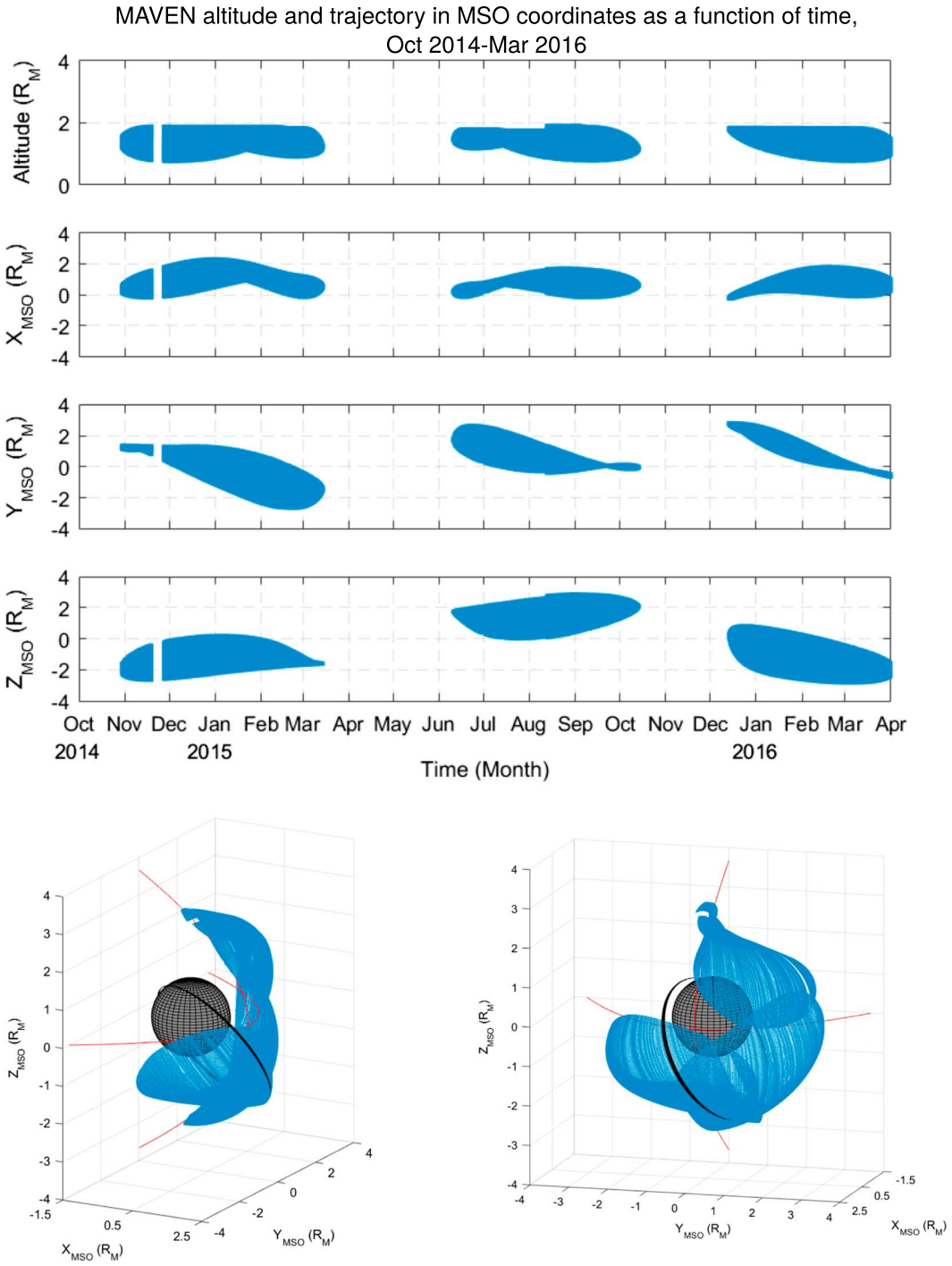

Figure 4. MAVEN spatial coverage of the region upstream from the Martian bow shock projected in MSO coordinates during the time interval 10 October 2014 to 31 March 2016 (bow shock fit taken from *Vignes et al.* [2000]). Each point corresponds to the mean position of an analyzed 10 min window. (first to fourth panels) SC altitude, X_{MSO}, Y_{MSO}, and Z_{MSO} coordinates as a function of time. (bottom panels) Three-dimensional spatial distribution of these points (in blue), together with the trajectory of MAVEN during ~ 2 days (in black). Red curves show the intersection between the Martian bow shock model and the $Z_{MSO} = 0$ and $Y_{MSO} = 0$ planes.

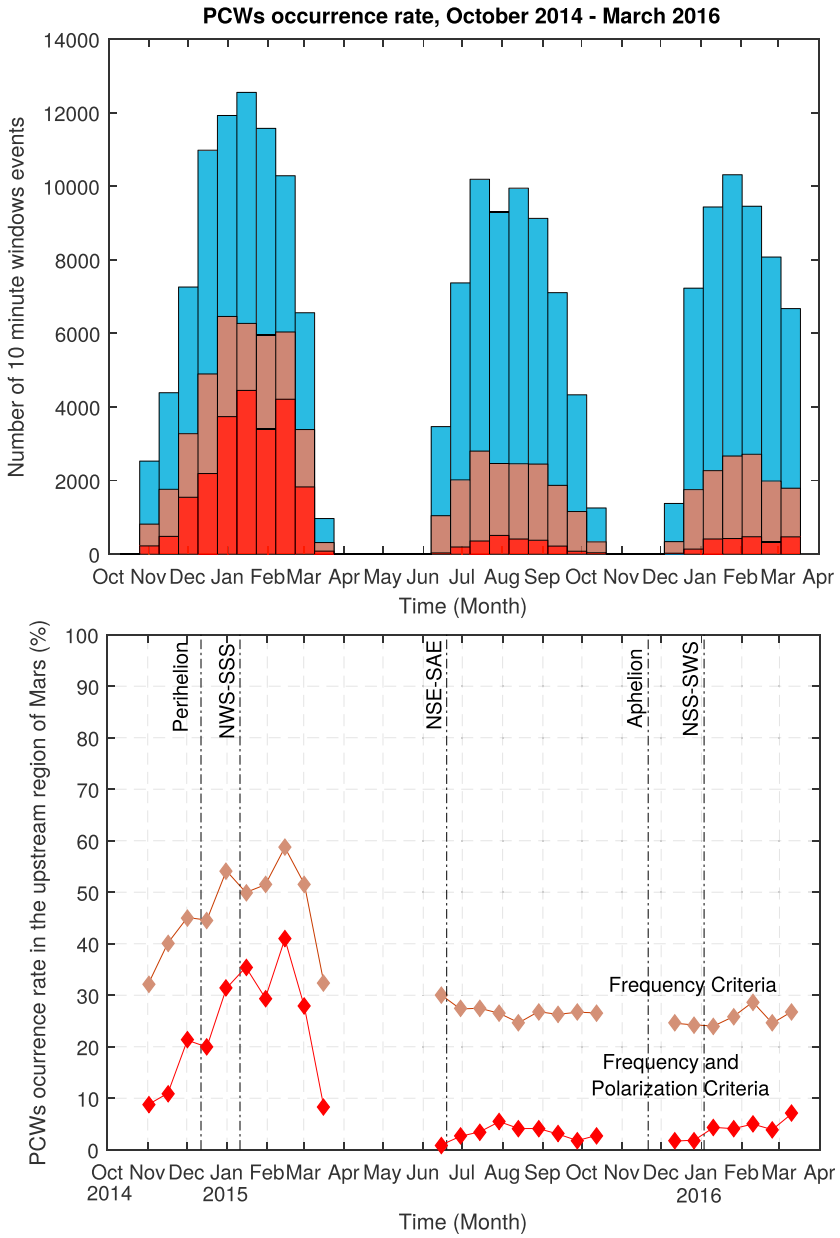

Figure 5. (top) Histograms of number of 10 min intervals studied as a function of time; blue: all analyzed 10 min intervals; brown: intervals with PCWs fulfilling first set of criteria; red: intervals with PCWs fulfilling also polarization criteria. (bottom) PCWs occurrence rate as a function of time, color coding as above. Northern Winter Solstice and Southern Summer Solstice (NWS-SSS), Northern Spring Equinox and Southern Autumn Equinox (NSE-SAE), and Northern Summer Solstice and Southern Winter Solstice (NSS-SWS) are also indicated.

observed to display changes [*Yamauchi et al.*, 2015]. The blue histogram displays the total number of these 10 min windows as a function of time, for all observation times (empty time intervals indicate lack of MAG data in the upstream region). The brown histogram is only for the intervals with PCWs fulfilling the first set of criteria on the PSD, the red histogram is for intervals with PCWs fulfilling also the second set of criteria, i.e., planar and left-hand polarized waves. Based on these histograms, Figure 5 (bottom) presents the PCWs occurrence rate in the upstream region of Mars as a function of time for both the frequential criteria (brown curve) and the frequential and polarization criteria combined (red curve). The vertical lines indicate for reference, and from left to right, the Martian PH, the NWS-SSS, the NSE-SAE, the Martian APH, and the NSS-SWS, respectively.

As can be seen in the blue histogram (Figure 5, top), the number of 10 min windows is approximately equally distributed along the whole time interval under study. The blue bin with the highest number contains ~10,000

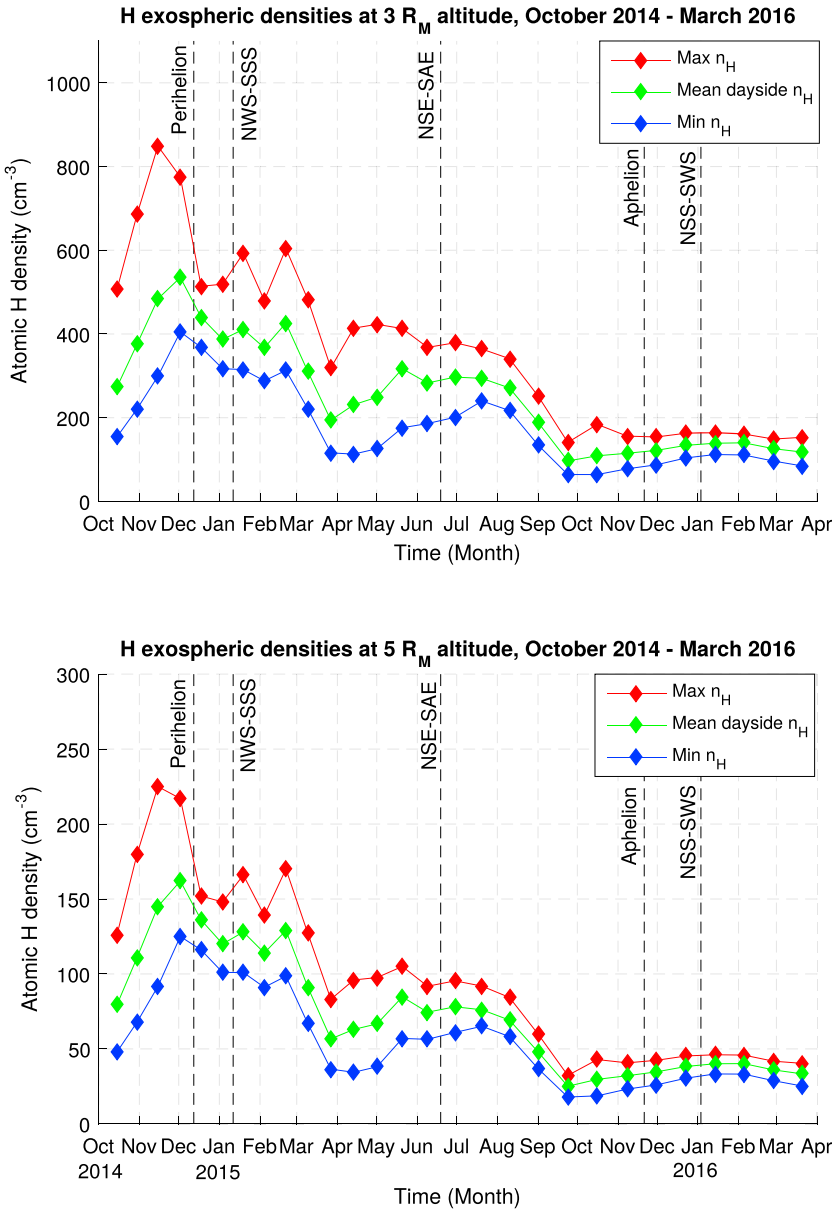

Figure 6. Simulated atomic H exospheric density as a function of time derived from the 3-D exospheric-LMD-GCM model, for two different altitudes upstream from the PCWs detection region: (top) 3 R_M and (bottom) 5 R_M, respectively.

10 min intervals, that with the lowest number (March–April 2015) still contains 966, sufficient to calculate the PCWs occurrence rate. Figure 5 (top) also clearly shows a (qualitative) decrease in the PCW occurrence rate when the brown and red bins for the same time intervals (with high number of 10 min intervals) are taken into consideration. In fact, the curves shown in Figure 5 (bottom) confirm this observation. Based on the frequency criteria (brown curve), we find that the PCWs occurrence rate is significantly higher around the Martian PH and NWS-SSS and takes much lower and constant values from the NSE-SAE up to the Martian APH and up to the end of March 2016. More precisely, PCW's occurrence rate takes values around 50% to 60% during January–March 2015, while their abundance is reduced to an average value around 25% for the SAE to March 2016 time interval. When the more strict criteria are applied (red curve), the overall abundance of PCWs is reduced as expected. However, the same clear contrast is still observed: during January–March 2015, there is a PCW's occurrence rate of 30–40%, while the abundance is reduced to an average value around 5% for the SAE to March 2016 time interval.

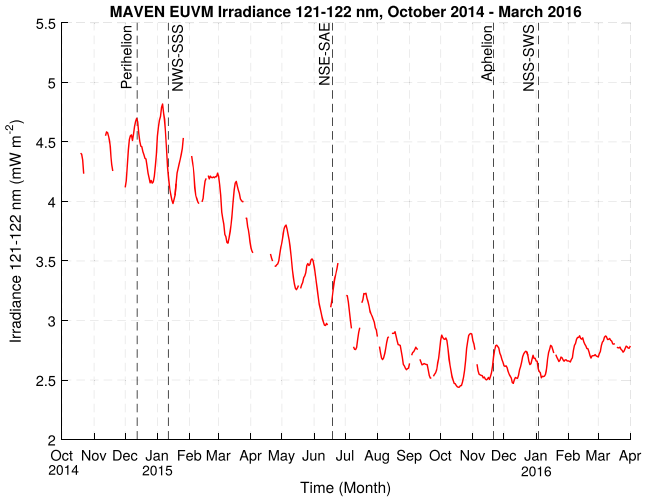

Figure 7. Daily irradiance in the wavelength range 121–122 nm measured by the MAVEN EUVM as a function of time.

In general, the main source of newborn pickup protons (capable of exciting PCWs) is the Martian H exosphere. MAVEN observes the PCWs at positions downstream of the source of the newborn ions, since the waves need time to grow and be convected to the observation position. Therefore, we study the H exosphere at higher altitudes using the 3-D exospheric-LMD-GCM numerical simulation model [*González-Galindo et al.*, 2009a; *Chaufray et al.*, 2012, 2015]. We derive atomic H exospheric densities for different Martian solar longitudes (taking averages over a 10° Martian solar longitude range), at different fixed altitudes. The latter are then converted to time using MAVEN ephemeris, obtaining then three estimations for the H atomic density (for a fixed altitude) per Martian month, approximately.

Figure 6 displays the calculated atomic H exospheric densities at the Martian dayside for ~3 R_M (top) and ~5 R_M (bottom), for the whole time interval and for mean solar conditions. These altitudes are chosen taking into account that pickup protons excite waves whose wavelengths are on the order of the Martian planetary radii [*Bertucci*, 2003]. Each panel shows maximum (red) , minimum (blue), and average (green) values. Higher H densities are obtained when Mars is near PH and the NWS-SSS, around the same time interval in which the PCWs occurrence rate is the highest. More precisely, H densities (at 3 R_M) around or higher than 350 cm^{-3} are mainly achieved between mid-November 2014 and March 2015. In contrast with this, H densities at 3 R_M hardly ever surpassed this value after the Martian NSE-SAE. Similarly for the case of H densities at 5 R_M, values around or higher than 100 cm^{-3} are mainly achieved between mid-November 2014 and March 2015, while this value is an upper limit after the Martian NSE-SAE.

One of the factors determining the temporal variability of the exospheric H density is the response of the Martian thermosphere to changes in the solar EUV flux reaching the planet. Interestingly, a similar behavior (to the long-term temporal variability of the simulated H density) is observed when analyzing irradiances in the 121–122 nm range obtained by MAVEN EUVM during the time interval under study (short compared to the solar cycle period). Figure 7 displays the daily average of the MAVEN EUVM measurements in that wavelength range as a function of time, providing then a proxy to study the temporal variability of the photoionization frequency of the neutral H exosphere. As it can be seen, the irradiance in the 121–122 nm wavelength range presents oscillations associated with the solar rotation period (~27 days) and decreases while the heliocentric distance of Mars increases. Indeed, the 121–122 nm daily irradiance takes values between 4.1 and 4.8 mW m^{-2} when Mars is between perihelion and the NWS-SSS, and it oscillates between 2.5 and 2.8 mW m^{-2} when Mars is between aphelion and the NSS-SWS. Both signatures, the increase in the maximum exospheric H density over the Martian day side as well the increase in the irradiance reaching Mars, take place when Mars is around PH. This then suggests an increase in the newborn proton (planetary) density around the same orbital position.

In addition to these analyses and in order to see if the observed long-term trend in the abundance of PCWs (Figure 5) could be the result of changes in MAVEN's altitude coverage or of temporal variations in the IMF orientation, we study the histograms for each of these parameters.

Figure 8 displays histograms with the normalized number of 10 min windows as a function of the SC altitude (in 0.1 R_M bins) separated in two time intervals: October 2014 to April 2015 (left) and June 2015 to March 2016 (right). These time intervals showed high abundance and low abundance of PCWs, respectively. The panels reveal that the SC coverage is not homogeneous in altitude since the SC spends more time near the apocenter of its elliptical orbit. Altitudes below 1.33 R_M are sampled with a low frequency (≤0.056); larger altitudes [1.33–1.73] R_M are sampled with higher frequency up to 0.130 (left) and 0.169 (right). There is a

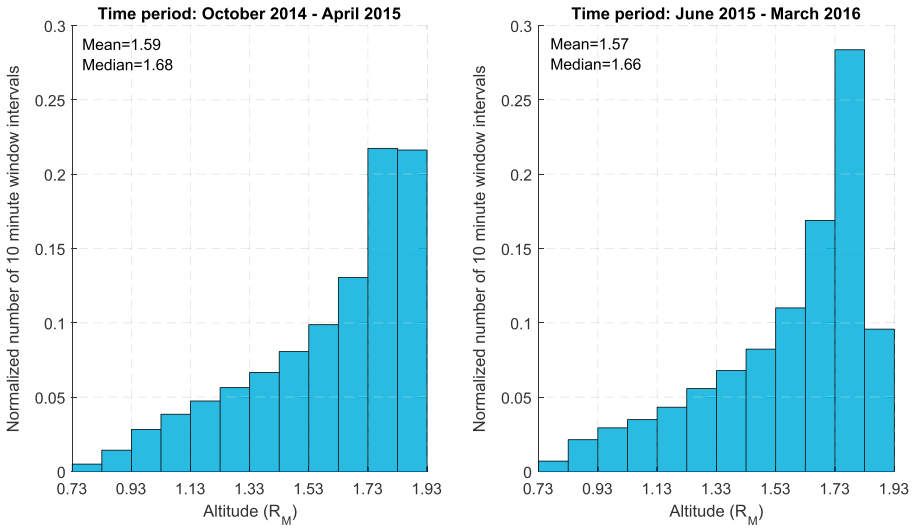

Figure 8. Normalized histograms of number of all 10 min intervals studied, as function of SC altitude. (left) Interval Oct 2014 to Apr 2015, where high PCW occurrences were found. (right) Interval Jun 2015 to Mar 2016, where low PCW occurrences were found.

difference in the highest altitude bins, but using a cumulative sampling frequency over the two bins, we obtain similar values: 0.22 (left) and 0.19 (right). The mean and median SC altitudes were also similar for both time intervals: 1.59 R_M and 1.68 R_M, respectively (left) and 1.57 R_M and 1.66 R_M, respectively (right). This comparison then suggests that temporal variabilities in MAVEN's altitude coverage cannot be the reason of the changes in the PCWs occurrence rate observed in Figure 5.

Theory indicates that the angle between the IMF and the SW velocity vector (for simplicity we consider that the latter is aligned with the X_{MSO} axis) determines the linear growth rate of the instabilities associated with the PCWs [*Gary*, 1993]. Therefore, we also analyze whether there are significant differences in the distribution of this angle between the time intervals with high and low PCWs occurrence rate. In analogy to Figure 8, Figure 9 displays two normalized histograms of the number of 10 min observation windows as function of θ_{BX} = angle ($\mathbf{B}$, $\mathbf{X}_{MSO}$) in bins of 10° width, for the time intervals with high (left) and low (right) PCWs occurrence. Any angle between 90° and 180° has been folded into this interval, since the parameter that affects the wave growth rate is the angle between the direction of both vectors and not the sense of them [see, e.g., *Gary*, 1993].

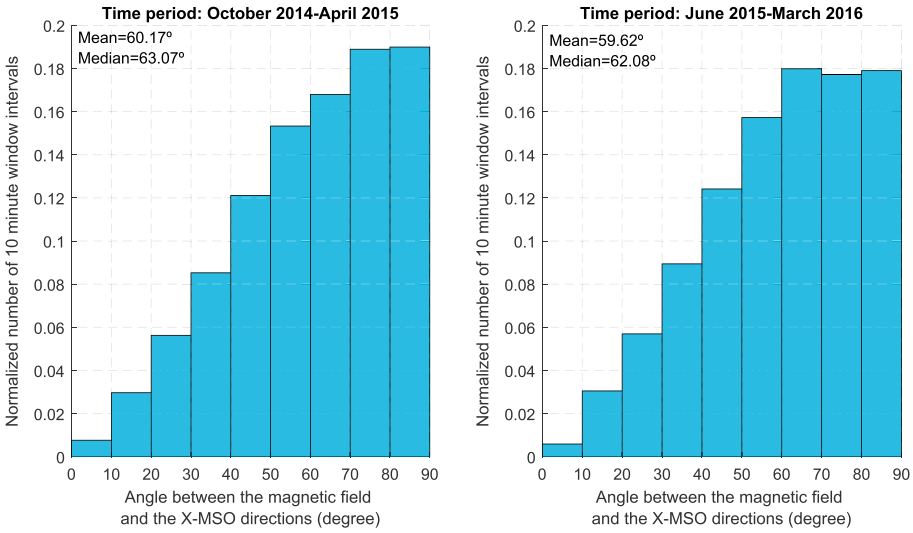

Figure 9. Normalized histograms of number of all 10 min intervals studied, as function of angle between magnetic field vector and SW flow direction. (left) Interval Oct 2014 to Apr 2015, where high PCW occurrences were found. (right) Interval Jun 2015 to Mar 2016, where low PCW occurrences were found.

As can be seen in both histograms, the angle $\mathbf{B} - X_{MSO}$ is also inhomogeneously covered. Indeed, a higher relative number of windows is found for higher θ_{BX}, but this is similar for both time intervals. Overall, a mean angle of 60.17° and a median angle of 63.07° is found in the October 2014 to April 2015 interval, while a mean angle of 59.62° and a median angle of 62.08° is derived for the June 2015 to March 2016 interval. Therefore, this comparison also suggests that temporal variabilities in the θ_{BX} angular distribution cannot be the reason for the observed changes in the PCWs occurrence rate as a function of time.

6. Discussion

The first main result of this study is the confirmation of the long-term trend previously reported in *Bertucci et al.* [2013], based on MGS MAG observations. In that study, the authors found that the occurrence rate of PCWs increases with decreasing distance of the planet to the Sun. As can be seen in Figure 5, we find that the occurrence of PCWs observed by MAVEN MAG between October 2014 and March 2016 increases when Mars is close to the PH and the NWS-SSS and remains relatively low and constant after the Martian NSE-SAE. The similarity in the long-term trend between both PCWs occurrence rate curves (brown and red) also suggests that the one based solely on PSD signatures do not contain a significant amount of fortuitous detection of waves without an exospheric origin (see, e.g., the discussion in *Mazelle and Neubauer* [1993]). Moreover, we also conclude that the increment in the PCWs occurrence rate cannot be the result of biases associated with MAVEN's spatial coverage of the upstream region. The X_{MSO} coverage, direction along which the PCWs are convected, does not show significant differences before and after the NSE-SAE, as shown in Figure 4 (second panel). The statistical distribution of the SC altitude also does not display significant changes between the time interval with high and low occurrence of PCWs (Figure 8). In spite of having sampled the $+Z_{MSO}$ hemisphere during the June 2015 to mid-October 2015 interval and the $-Z_{MSO}$ hemisphere during the mid-December 2015 to March 2016 interval, we found a very low occurrence of PCWs in both cases. In contrast, we found high occurrence of waves in the southern hemisphere when Mars was around PH, suggesting then that the differences in the spatial distribution of the crustal magnetic fields does not have an appreciable effect in the existence of these waves. Moreover, this also suggests that the observed temporal variations are mainly driven by the Martian heliocentric distance rather than the seasons. Also, the observed changes in the PCW's occurrence rate cannot be associated to changes in the angle between the background magnetic field and the SW velocity direction. As seen from Figure 9, the statistical distribution of this parameter does not show significant differences before and after the Martian NSE-SAE. Additionally, to evaluate the impact of the variability of the Martian bow shock location on the results presented in Figure 5, we perform analogous PCW estimations taking into account the statistical variability observed in the MGS bow shock crossings [*Vignes et al.*, 2000]. These complementary estimations do no show meaningful differences compared with the statistical results presented in this work.

Interestingly, observational evidence of a strong seasonal dependence in the hydrogen exosphere of Mars has been recently reported in *Clarke et al.* [2014], *Chaffin et al.* [2014], and *Bhattacharyya et al.* [2015], based on Hubble Space Telescope and MEX scattered Lyman α brightness observations. In agreement with these observations, a large decrease in the median penetrating proton density [*Halekas et al.*, 2016] derived from MAVEN Solar Wind Ion Analyzer (SWIA) [*Halekas et al.*, 2015] measurements is observed during the MAVEN mission (lower density values for larger heliocentric distances) and also indicates a high level of seasonal variability in the Martian H exosphere. Concerning this point, we find that the temporal variability of the simulated H exospheric densities (under solar mean conditions) displays a similar behavior to that observed in the PCWs occurrence rate. Indeed, seasonal variations of the H density in the exosphere are, in general, driven by the variations of the temperature and the H density at the exobase. However, between 10,000 km and 20,000 km the effect of the temperature at the exobase is dominant, leading to a maximal average exospheric density near perihelion and a minimum density near aphelion, as shown in Figure 6. The simulation results also suggest that the dayside Martian H exosphere is not isotropic at these altitudes. Moreover, the dayside variability (at these altitudes) for a given time (associated with a given Martian solar longitude) depends on the seasons. This is the case, for example, for the locations of the maximum and minimum of the H density which depend on the conditions (complex patterns) at the exobase [see, e.g., *Chaufray et al.*, 2015]. Near equinoxes, the density is found to be maximum close to the subsolar region, while at other time intervals there is a north/south asymmetry resulting from a north/south asymmetry distribution at the exobase, enhanced when a narrow region near one geographic pole is permanently in the nightside. In the latter case, this region is hydrogen rich

due to the descent of air from the equatorial to the polar region (for more information on the wind-induced diffusion, see, for example, *Bougher et al.* [2015]), also responsible for the polar warming [*González-Galindo et al.*, 2009b]. At the exobase H densities can vary by more than 1 order of magnitude, but this asymmetry is reduced at higher altitudes in the exosphere.

Additionally, daily irradiances in the 121 – 122 nm wavelength range measured by MAVEN EUVM clearly display a long-term trend with increasing intensity when the Sun-Mars distance decreases (Figure 7), thus suggesting an increase in the photoionization frequency of the exospheric H atoms. As stated above, the upper H exosphere is mainly controlled by the averaged temperature at the exobase, which is UV dependent [*Chaufray et al.*, 2015]. Temporal variabilities in the simulated H densities (Figure 6) partly arise as a result of the Martian thermospheric response to changes in the UV flux associated with variations in the heliocentric distance. In this regard, such behavior is also consistent with the daily irradiances derived from EUVM observations.

All the previous results are then in favor of a correlation between the state of the Martian upper exosphere and the presence or absence of the analyzed waves. Indeed, the plasma instability giving rise to the PCWs observed by MAVEN depends, among other factors, on the density of newborn planetary protons implanted into the SW, which, in turn, varies (among other factors) in response to changes in the solar EUV flux reaching Mars. The solar EUV flux reaching Mars varies not only as a result of changes in the solar activity (longer time scales than the ones involved in this work) but also as a result of changes in the heliocentric distance of Mars and the Sun's rotation, as shown in Figure 7. Changes in the EUV flux can lead to changes in the photoionization frequencies of the Martian exosphere. However, they can also influence the state of the Martian thermosphere, which additionally affects the atomic H density profiles even at exospheric altitudes, affecting, in turn, the amount of newborn ions that can be generated by photoionization as well as charge exchange.

Seasonal changes in the detection probability of planetary newborn protons in the upstream region of Mars have been observed by MEX during 8 Earth years. Such variabilities also include a north-south asymmetry, although much smaller than the (perihelion-aphelion) distance effect [*Yamauchi et al.*, 2015]. Therefore, these large amounts of plasma measurements provide additional support to the interpretation proposed to explain the long-term temporal variabilities observed in the abundance of PCWs. These authors also determined that the relative changes observed in the pickup ion fluxes cannot totally be explained in terms of relative changes in EUV fluxes reaching at Mars. Consequently, *Yamauchi et al.* [2015] concluded that even though the variation in solar UV flux has a major effect on the formation of pickup ions, it is not the only contributing component. Similarly, *Bhattacharyya et al.* [2015] also concluded that the observed seasonal changes in the neutral H exospheric densities cannot be explained only on the basis of changes in the incident EUV flux. Moreover, the supplying process of H to the exosphere of Mars through diffusion of molecular H_2 from lower altitudes is slow, not capable of explaining observed short-term changes in the H density. In light of this, *Bhattacharyya et al.* [2015] suggested that effects associated with high concentrations of water vapor in the lower atmosphere could lead to fast changes in the H component of the exosphere, and therefore, it could be at least one of the missing contributing factors for the H seasonal changes. Such high concentrations of water vapor in the lower atmosphere were observed by MEX, as shown in *Fedorova et al.* [2006, 2009] and *Maltagliati et al.* [2011, 2013]. In this sense, a future study on the effects that this component may have in the upper H exospheric densities can help to improve the understanding of the dynamics of the Martian exosphere, and therefore, it could also provide a more clear correlation with the presence or absence of PCWs closer to the planet. Additionally, a study on the relationship between the properties of the proton velocity distribution functions upstream from the bow shock (observed by MAVEN SWIA and STATIC [*McFadden et al.*, 2015]) and that of PCWs should also be undertaken.

Finally, it is worth mentioning that changes in the abundances of PCWs are not a unique feature of the Martian environment. By analyzing and comparing Venus Express MAG and ASPERA data during 2 Venus years under solar maximum and solar minimum conditions, *Delva et al.* [2015] reported significant differences in the PCWs occurrence rate between both time intervals. The higher number of PCWs events observed near solar maximum were associated with a higher relative density of planetary exospheric protons with respect to the background SW proton density in this time interval.

7. Conclusions

Through this study, performed for the time interval from October 2014 to March 2016, we find that the presence of PCWs as observed by MAVEN MAG is significantly higher when Mars is close to perihelion and takes

lower and relatively constant values from the Northern Spring Equinox-Southern Autumn Equinox up to the end of the studied time interval. We also conclude that these variabilities are not the result of biases associated with the spatial coverage of MAVEN or with changes in the orientation of the background magnetic field. We do find, however, a clearly correlated behavior with the temporal changes of the simulated H exospheric densities upstream from the PCWs detection spatial region. These variabilities are partly due to differences in the response of the Martian thermosphere for different values of UV flux reaching Mars at different heliocentric distances, also observed in the daily irradiances measured by MAVEN EUVM. Particularly, higher simulated H densities as well as observed daily irradiances are found near perihelion. This then suggests an increase in the amount of newborn planetary protons implanted into the solar wind upstream from the bow shock of Mars, which are presumed to be the original source for the observed PCWs.

Future analyses on the relationship between temporal variabilities in the PCWs occurrence rate upstream from the Martian bow shock and that of H exospheric densities would benefit from studies on the observed properties of proton velocity distribution functions in this region. Additional studies on the effects that high concentrations of water vapor in the lower atmosphere may have on the exospheric H density could also help to understand better the coupling between the Martian neutral exosphere and the abundance of these low-frequency electromagnetic plasma waves. More generally, these two approaches can improve the possibilities to indirectly monitor the temporal variability of the upper H exosphere over long scales, depending on the occurrence rate of PCWs.

Acknowledgments

N.R. is supported by a CDD contract from CNES. MAVEN data are publicly available through the Planetary Data System. Please contact J-Y. Chaufray (Jean-Yves.Chaufray@latmos.ipsl.fr) for access to the LMD-GCM and exospheric numerical simulations used in this article. N.R. thanks Emmanuel Penou for all his help during the present study.

References

Acuña, M. H., et al. (1998), Magnetic field and plasma observations at Mars: Initial results of the Mars Global Surveyor mission, *Science*, *279*(5357), 1676–1680, doi:10.1126/science.279.5357.1676.

Albee, A. L., R. E. Arvidson, F. Palluconi, and T. Thorpe (2001), Overview of the Mars Global Surveyor mission, *J. Geophys. Res.*, *106*(E10), 23,291–23,316, doi:10.1029/2000JE001306.

Bhattacharyya, D., J. T. Clarke, J.-L. Bertaux, J.-Y. Chaufray, and M. Mayyasi (2015), A strong seasonal dependence in the Martian hydrogen exosphere, *Geophys. Res. Lett.*, *42*, 8678–8685, doi:10.1002/2015GL065804.

Bertucci, C. (2003), Étude de l'interaction du vent solaire avec Mars: Implications sur les mécanismes d'échappement atmosphérique, Thèse de doctorat, Univ. Paul Sabatier. [Available at https://hal.inria.fr/file/index/docid/48559/filename/tel-00010454.pdf.]

Bertucci, C., N. Romanelli, J. Y. Chaufray, D. Gomez, C. Mazelle, M. Delva, R. Modolo, F. González-Galindo, and D. A. Brain (2013), Temporal variability of waves at the proton cyclotron frequency upstream from Mars: Implication for Mars distant hydrogen exosphere, *Geophys. Res. Lett.*, *40*, 3809–3813, doi:10.1002/grl.50709.

Brain, A., et al. (2002), Observations of low-frequency electromagnetic plasma waves upstream from the Martian shock, *J. Geophys. Res.*, *107*(A6), 1076, doi:10.1029/2000JA000416.

Brain, D. A., J. S. Halekas, R. Lillis, D. L. Mitchell, R. P. Lin, and D. H. Crider (2005), Variability of the altitude of the Martian sheath, *Geophys. Res. Lett.*, *32*, L18203, doi:10.1029/2005GL023126.

Brinca, A., and B. T. Tsurutani (1989), Influence of multiple ion species on low-frequency electromagnetic wave instabilities, *J. Geophys. Res.*, *94*, 13,565–13,569.

Brinca, A. (1991), Cometary linear instabilities: From profusion to perspertive in Cometary Plasma Processes, *Geophys. Monograph*, *61*, 211–221.

Bougher, S. W., D. Pawlowski, J. M. Bell, S. Nelli, T. McDunn, J. R. Murphy, M. Chizek, and A. Ridley (2015), Mars Global Ionosphere-Thermosphere Model (MGITM): Solar cycle, seasonal, and diurnal variations of the Mars upper atmosphere, *J. Geophys. Res. Planets*, *120*, 311–342, doi:10.1002/2014JE004715.

Chaffin, M. S., J.-Y. Chaufray, I. Stewart, F. Montmessin, N. M. Schneider, and J.-L. Bertaux (2014), Unexpected variability of Martian hydrogen escape, *Geophys. Res. Lett.*, *41*, 314–320, doi:10.1002/2013GL058578.

Chaffin, M. S., et al. (2015), Three-dimensional structure in the Mars H corona revealed by IUVS on MAVEN, *Geophys. Res. Lett.*, *42*, 9001–9008, doi:10.1002/2015GL065287.

Chaufray, J. Y., J. L. Bertaux, F. Leblanc, and E. Quémerais (2008), Observation of the hydrogen corona with SPICAM on Mars Express, *Icarus*, *195*(2), 598–613.

Chaufray, J.-Y., et al. (2012), *Current Status on Mars Exospheric Studies*, Mysore, India.

Chaufray, J.-Y., F. Gonzalez-Galindo, F. Forget, M. A. Lopez-Valverde, F. Leblanc, R. Modolo, and S. Hess (2015), Variability of the hydrogen in the Martian upper atmosphere as simulated by a 3D atmosphere-exosphere coupling, *Icarus*, *245*, 282–294, doi:10.1016/j.icarus.2014.08.038.

Clarke, J. T., J.-L. Bertaux, J.-Y. Chaufray, G. R. Gladstone, E. Quemerais, J. K. Wilson, and D. Bhattacharyya (2014), A rapid decrease of the hydrogen corona of Mars, *Geophys. Res. Lett.*, *41*, 8013–8020, doi:10.1002/2014GL061803.

Convery, P., and P. Gary (1997), Electromagnetic proton cyclotron ring instability: Threshold and saturation, *J. Geophys. Res.*, *102*(A2), 2351–2358.

Connerney, J. E. P., J. R. Espley, G. A. DiBraccio, J. R. Gruesbeck, R. J. Oliversen, D. L. Mitchell, J. Halekas, C. Mazelle, D. Brain, and B. M. Jakosky (2015a), First results of the MAVEN magnetic field investigation, *Geophys. Res. Lett.*, *42*, 8819–8827, doi:10.1002/2015GL065366.

Connerney, J. E. P., J. Espley, P. Lawton, S. Murphy, J. Odom, R. Oliversen, and D. Sheppard (2015b), The MAVEN magnetic field investigation, *Space Sci. Rev.*, *195*, 1–35, doi:10.1007/s11214-015-0169-4.

Cowee, M. M., et al. (2012), Pickup ions and ion cyclotron wave amplitudes upstream of Mars: First results from the 1D hybrid simulation, *Geophys. Res. Lett.*, *39*, L08104, doi:10.1029/2012GL051313.

Delva, M., C. Bertucci, M. Volwerk, R. Lundin, C. Mazelle, and N. Romanelli (2015), Upstream proton cyclotron waves at Venus near solar maximum, *J. Geophys. Res. Space Physics*, *120*, 344–354, doi:10.1002/2014JA020318.

Eparvier, F. G., P. C. Chamberlin, T. N. Woods, and E. M. B. Thiemann (2015), The solar extreme ultraviolet monitor for MAVEN, *Space Sci. Rev.*, 1–9.

Fedorova, A., O. Korablev, J.-L. Bertaux, A. Rodin, A. Kiselev, and S. Perrier (2006), Mars water vapor abundance from SPICAM IR spectrometer: Seasonal and geographic distributions, *J. Geophys. Res.*, *111*, E09S08, doi:10.1029/2006JE002695.

Fedorova, A., O. I. Korablev, J.-L. Bertaux, A. V. Rodin, F. Montmessin, D. A. Belyaev, and A. Reberac (2009), Solar infrared occultation observations by SPICAM experiment on Mars-Express: Simultaneous measurements of the vertical distributions of H_2O, CO_2 and aerosol, *Icarus*, *200*, 96–117.

Gary, S. P., and C. Madland (1988), Electromagnetic ion instabilities in a cometary environment, *J. Geophys. Res.*, *93*(A1), 235–241.

Gary, S. P., K. Akimoto, and D. Winske (1989), Computer simulations of cometary ion/ion instabilities and wave growth, *J. Geophys. Res.*, *94*(A4), 3513–3525.

Gary, S. P. (1991), Electromagnetic ion/ion instabilities and their consequences in space plasmas: A review, *Space Sci. Rev.*, *56*, 373–415.

Gary, S. P. (1993), *Theory of Space Plasma Microinstabilities*, Cambridge Atmospheric and Space Series, Cambridge Univ. Press, Cambridge.

González-Galindo, F., M. A. Lopez-Valverde, M. A. Angelats i Coll, and F. Forget (2005), Extension of a Martian general circulation model to thermospheric altitudes: UV heating and photochemical models, *J. Geophys. Res.*, *110*, E09008, doi:10.1029/2004JE002312.

González-Galindo, F., et al. (2009a), A ground-to-exosphere Martian circulation model: 1. Seasonal, diurnal, and solar cycle variation of thermospheric temperatures, *J. Geophys. Res.*, *114*, E04001, doi:10.1029/2008JE003246.

González-Galindo, F., F. Forget, M. A. López-Valverde, and M. Angelats i Coll (2009b), A ground-to-exosphere Martian circulation model: 2. Atmosphere during solstice conditions—Thermospheric polar warming, *J. Geophys. Res.*, *114*, E08004, doi:10.1029/2008JE003277.

Halekas, J. S., E. R. Taylor, G. Dalton, G. Johnson, D. W. Curtis, J. P. McFadden, D. L. Mitchell, R. P. Lin, and B. M. Jakosky (2015), The solar wind ion analyzer for MAVEN, *Space. Sci. Rev.*, doi:10.1007/s11214-013-0029-z.

Halekas, J. S., et al. (2016), Structure, dynamics, and seasonal variability of the Mars-solar wind interaction: MAVEN solar wind ion analyzer inflight performance and science results, *J. Geophys. Res. Space Physics*, *121*, doi:10.1002/2016JA023167.

Jakosky, B. M., et al. (2015), The Mars Atmosphere and Volatile EvolutioN (MAVEN) mission, *Space Sci. Rev.*, *195*, 3–48, doi:10.1007/s11214-015-0139-x.

McFadden, J., et al. (2015), The MAVEN Suprathermal and thermal Ion Composition (STATIC) Instrument, *Space Sci. Rev.*, *195*, 199–256.

Maltagliati, L., F. Montmessin, A. Fedorova, O. Korablev, F. Forget, and J.-L. Bertaux (2011), Evidence of water vapor in excess of saturation in the atmosphere of Mars, *Science*, *333*, 1868–1871.

Maltagliati, L., F. Montmessin, O. Korablev, A. Fedorova, F. Forget, A. Määttänen, F. Lefèvre, and J.-L. Bertaux (2013), Annual survey of water vapor vertical distribution and water aerosol coupling in the Martian atmosphere observed by SPICAM/MEX solar occultations, *Icarus*, *223*, 942–862.

Mazelle, C., and F. M. Neubauer (1993), Discrete wave packets at the proton cyclotron frequency at Comet P/Halley, *Geophys. Res. Lett.*, *20*, 153–156.

Mazelle, C., et al. (2004), Bow shock and upstream phenomena at Mars, *Space Sci. Rev.*, *111*, 115–181.

Romanelli, N., C. Bertucci, D. Gomez, C. Mazelle, and M. Delva (2013), Proton cyclotron waves upstream from Mars: Observations from Mars global surveyor, *Planet. Space Sci.*, *76*, 1–9.

Ruhunusiri, S., J. S. Halekas, J. E. P. Connerney, J. R. Espley, J. P. McFadden, D. E. Larson, D. L. Mitchell, C. Mazelle, and B. M. Jakosky (2015), Low-frequency waves in the Martian magnetosphere and their response to upstream solar wind driving conditions, *Geophys. Res. Lett.*, *42*, 8917–8924, doi:10.1002/2015GL064968.

Ruhunusiri, S., et al. (2016), MAVEN observation of an obliquely propagating low-frequency wave upstream of Mars, *J. Geophys. Res. Space Physics*, *121*, 2374–2389, doi:10.1002/2015JA022306.

Russell, C. T., et al. (1990), Upstream waves at Mars—PHOBOS observations, *Geophys. Res. Lett.*, *17*(6), 897–900.

Sauer, K., E. Dubinin, and J. F. McKenzie (2001), New type of soliton in Bi-ion plasmas and possible implications, *Geophys. Res. Lett.*, *28*, 3589–3592, doi:10.1029/2001GL013047.

Sauer, K., and E. Dubinin (2003), Oscillitons and gyrating ions in a beam-plasma system, *Geophys. Res. Lett.*, *30*, 2192, doi:10.1029/2003GL018266.

Sonnerup, B. U. Ö., and M. Scheible (1998), Minimum and maximum variance analysis, in *Analysis Methods for Multi-Spacecraft Data*, ISSI Scientific Reports Series, vol. 1, pp. 185–220, edited by G. Paschmann and P. Daly, ESA Publications Division, Noordwijk, Netherlands.

Tsurutani, B. T., et al. (1989), Magnetic pulses with durations near the local proton cyclotron period: Comet Giacobini-Zinner, *J. Geophys. Res.*, *94*, 29–35.

Tsurutani, B. T. (1991), Comets: A laboratory for plasma waves and instabilities, in *Cometary Plasma Processes, Geophys. Monogr. Ser.*, vol. 61, pp. 189–209, AGU, Washington, D. C.

Vignes, D., C. Mazelle, H. Reme, M. H. Acuña, J. E. P. Connerney, R. P. Lin, D. L. Mitchell, P. Cloutier, D. H. Crider, and N. F. Ness (2000), The solar wind interaction with Mars: Locations and shapes of the bow shock and the magnetic pile-up boundary from the observations of the MAG/ER experiment onboard Mars global surveyor, *Geophys. Res. Lett.*, *27*(1), 49–52, doi:10.1029/1999GL010703.

Wei, H., and C. T. Russell (2006), Proton cyclotron waves at Mars: Exosphere structure and evidence for a fast neutral disk, *J. Geophys. Res.*, *33*, L23103, doi:10.1029/2006GL026244.

Wei, H. Y., C. T. Russell, T. L. Zhang, and X. Blanco-Cano (2011), Comparative study of ion cyclotron waves at Mars, Venus and Earth, *Planet. Space Sci.*, *59*, 1039–1047.

Wei, H. Y., M. M. Cowee, C. T. Russell, and H. K. Leinweber (2014), Ion cyclotron waves at Mars: Occurrence and wave properties, *J. Geophys. Res. Space Physics*, *119*, 5244–5258, doi:10.1002/2014JA020067.

Wu, C. S., and R. C. Davidson (1972), Electromagnetic instabilities produced by neutral-particle ionization in interplanetary space, *J. Geophys. Res.*, *77*(28), 5399–5406, doi:10.1029/JA077i028p05399.

Wu, C. S., and R. E. Hartle (1974), Further remarks on plasma instabilities produced by ions born in the solar wind, *J. Geophys. Res.*, *79*, 283–285.

Yamauchi, M., et al. (2015), Seasonal variation of Martian pick-up ions: Evidence of breathing exosphere, *Planet. Space Sci.*, *119*, 54–61, doi:10.1016/j.pss.2015.09.013.